Nano Energy 81 (2021) 105570

Contents lists available at ScienceDirect

Nano Energy

journal homepage: http://www.elsevier.com/locate/nanoen

Full paper

Highly-efficient all-inorganic lead-free 1D $CsCu_2I_3$ single crystal for white-light emitting diodes and UV photodetection

Xiaoming Mo [a,1], Tao Li [a,1], Fengchang Huang [a], Zhuxin Li [b], Yulu Zhou [a], Tao Lin [a], Yifang Ouyang [a], Xiaoma Tao [a,*], Caofeng Pan [c,*]

[a] Center on Nanoenergy Research, School of Physical Science and Technology, Guangxi University, Nanning 530004, People's Republic of China
[b] State Key Laboratory of Bioelectronics, School of Biological Science & Medical Engineering, Southeast University, Nanjing 210096, People's Republic of China
[c] Beijing Institute of Nanoenergy and Nanosystems, Chinese Academy of Sciences, Beijing 100083, People's Republic of China

ARTICLE INFO

Keywords:
Lead-free
Copper(I)
Perovskite
Light-emitting diodes
Photodetector

ABSTRACT

Lead-based halide perovskites have received great research interest in producing exceptional optoelectronic devices owing to their superior photophysical properties. However, inclusion of toxic Pb in these perovskites brings great risk to public health and hinders their use. Here we report the use of copper(I) to fully substitute Pb to produce Pb-free one-dimensional (1D) $CsCu_2I_3$ single crystals (SCs). High-quality, air stable, and yellow-emitting 1D $CsCu_2I_3$ SC with length as long as 13 mm is synthesized via inverse temperature crystallization method. A record photoluminescence quantum yield (PLQY) first exceeding 50% (50.4%) is obtained with oleic acid as additive during growth. White light-emitting diodes produced by using the 1D $CsCu_2I_3$ SC as yellow phosphors are strikingly capable of working continuously for more than 580 h with a half-lifetime of ~150 h in air. Photodetectors fabricated by the 1D $CsCu_2I_3$ SC show distinct UV response with fast response time as low as 50.4 ms (at 340 nm). Our findings pave a way by using the copper(I)-based 1D $CsCu_2I_3$ SCs for future high-efficiency solid-state lighting and fast UV photodetection applications.

1. Introduction

Over the last few years, 3D lead halide perovskites have risen as attractive materials to produce optoelectronic devices owing to their excellent photophysical properties [1,2]. State-of-the-art photovoltaic cells, light-emitting diodes (LEDs), nano lasers, and photodetectors (PDs) based on the 3D perovskites have been proposed and fabricated in the past few years [3–6]. Recently, low-dimensional 2D/1D/0D perovskites have also attracted considerable attentions due to their intrinsic quantum-confinement-induced high exciton binding energies and high photoluminescence quantum yields (PLQYs). The high exciton binding energies guarantee the stability of the excitons at room temperature (RT) or higher temperatures, leading the PLQYs of the 2D/1D/0D perovskites up to as high as near unity (such as $PEA_2(CH_3NH_3)_{n-1}Pb_nI_{3n+1}$ [7], $NFPbI_7$ [8], $C_4N_2H_{14}PbBr_4$ [9], Cs_4PbBr_6 [10,11], $CsPbX_3$ [12–14], *etc.*). Despite the high PLQYs in these perovskites, nevertheless, the toxicity of Pb is becoming a risky issue that needs to be addressed before mass commercialization due to its severe harms to children and environment. Fully substituting Pb with nontoxic divalent cations is proposed to address this issue (using Sn^{2+}, Ge^{2+}, Sb^{3+}, Bi^{3+}, Cu^{2+}, *etc.*) because of the simplicity and effectiveness of the synthesis by preserving the perovskite structure [15]. However, these approaches are still far from satisfaction because of either the low PLQYs or the instability induced by the organic cations [16]. In consideration of these facts, caesium-based all-inorganic double perovskites were also proposed and demonstrated lately to show high quantum efficiencies and high PL stability by fully replacing two Pb cations with a trivalent metal cation as well as a monovalent metal cation to form $Cs_2M^IM^{III}X_6$ (M^I = Ag, Na, and K; M^{III} = In, Sb and Bi; X = Cl, Br and I) [17–23]. Unfortunately, in general, bandgaps of the double perovskites reported currently are either too large or are indirect to be suitable for producing high-efficiency optoelectronic devices. Furthermore, inclusion of heavy and/or noble metal cations (like Bi^{3+}, In^{3+} and Ag^{+}) might not be favorable for the further development of the lead-free double perovskites. Hence, novel nontoxic cations are highly needed to design the all-inorganic lead-free halide materials to promote the stability and

* Corresponding authors.
E-mail addresses: taoxiaoma@gxu.edu.cn (X. Tao), cfpan@binn.cas.cn (C. Pan).
[1] These authors contributed equally to this work.

https://doi.org/10.1016/j.nanoen.2020.105570
Received 26 September 2020; Received in revised form 2 November 2020; Accepted 2 November 2020
Available online 14 November 2020

quantum efficiency.

Most recently, copper(I) has been proposed to fully substitute Pb to produce all-inorganic lead-free halide emitters $(CsX)_{1-y}(CuX)_y$ (X=I, Br, and Cl), resulting in a new halide material family for optoelectronic applications without perovskite crystal structures [24–34]. Ultra-high quantum efficiencies (near unity) with exceptional air stability over 2 months were obtained from such Cu(I)-based halides. The formation of 0D electronic structure with $[Cu_2I_5]^{3-}$ as the photoactive site and Cs^+ ions as the isolator gave an exciton binding energy of ~490 meV and PLQYs as high as 90% for single crystals (SCs) and 60% for thin films [24]. It was also reported that it might be the Cu(I) ions that played a crucial role for the bright emission of the Cu(I)-based halides, rather than other monovalent ion like Ag^+ [35]. These results suggested that Cu(I)-based halides can be promising to produce high-efficiency light emitters for outstanding optoelectronic applications. On the basis of crystal structures of the $(CsX)_{1-y}(CuX)_y$, a material family of Cu(I)-based ternary halide compounds may be obtained with increasing the Cu composition (improving y): Cs_2CuX_3, $Cs_3Cu_2X_5$, $CsCuX_2$, $CsCu_2X_3$, $CsCu_4X_5$, and $CsCu_9X_{10}$ (X = Cl, Br, and I) [36]. Although some of these Cu(I)-based halides like $Cs_3Cu_2I_5$ and $Cs_3Cu_2Br_5$ have been reported to show high PLQYs and stability [24,25], researches on the other sub-families of these Cu(I)-based halides are just beginning and their photophysical properties have not been well revealed yet [37–40]. Most importantly, the reported Cu(I)-based halides with high efficiencies are generally blue or green emissive. For the halides that generate longer yellow or red wavelength emissions, the efficiency is still very low (< 20.6%) and far from satisfaction. Hence, for potential full-color display and solid-state lighting applications, novel copper(I)-based halides that efficiently generate the longer wavelength is highly required to match the high efficiencies of the blue or green copper(I) halides.

In this work, focusing on the sub-family of $CsCu_2X_3$ halide, we have synthesized and demonstrated Cu(I)-based 1D $CsCu_2I_3$ SC with length as long as 13 mm by using inverse temperature crystallization (ITC) method, rather than using antisolvent vapor-assisted crystallization (AVC) methods as reported previously. The 1D $CsCu_2I_3$ SC has high quality and shines single-band bright yellow emission at 580 nm with a champion PLQY as high as 50.4%. The 1D $CsCu_2I_3$ SC shows high thermal stability up to 480 °C and ultra-high PL stability after being stored in ambient air with RH of 40% for over 2,200 h. White LEDs (WLEDs) produced by using the bright yellow emitting 1D $CsCu_2I_3$ SC as yellow phosphors of UV LEDs strikingly exhibit bright white-light emission for more than 580 h with a half-lifetime (L_{50}) of ~150 h in air under a continuously driving current of 50 mA. PDs fabricated by the 1D $CsCu_2I_3$ SC show distinct UV response at 365 nm with fast response

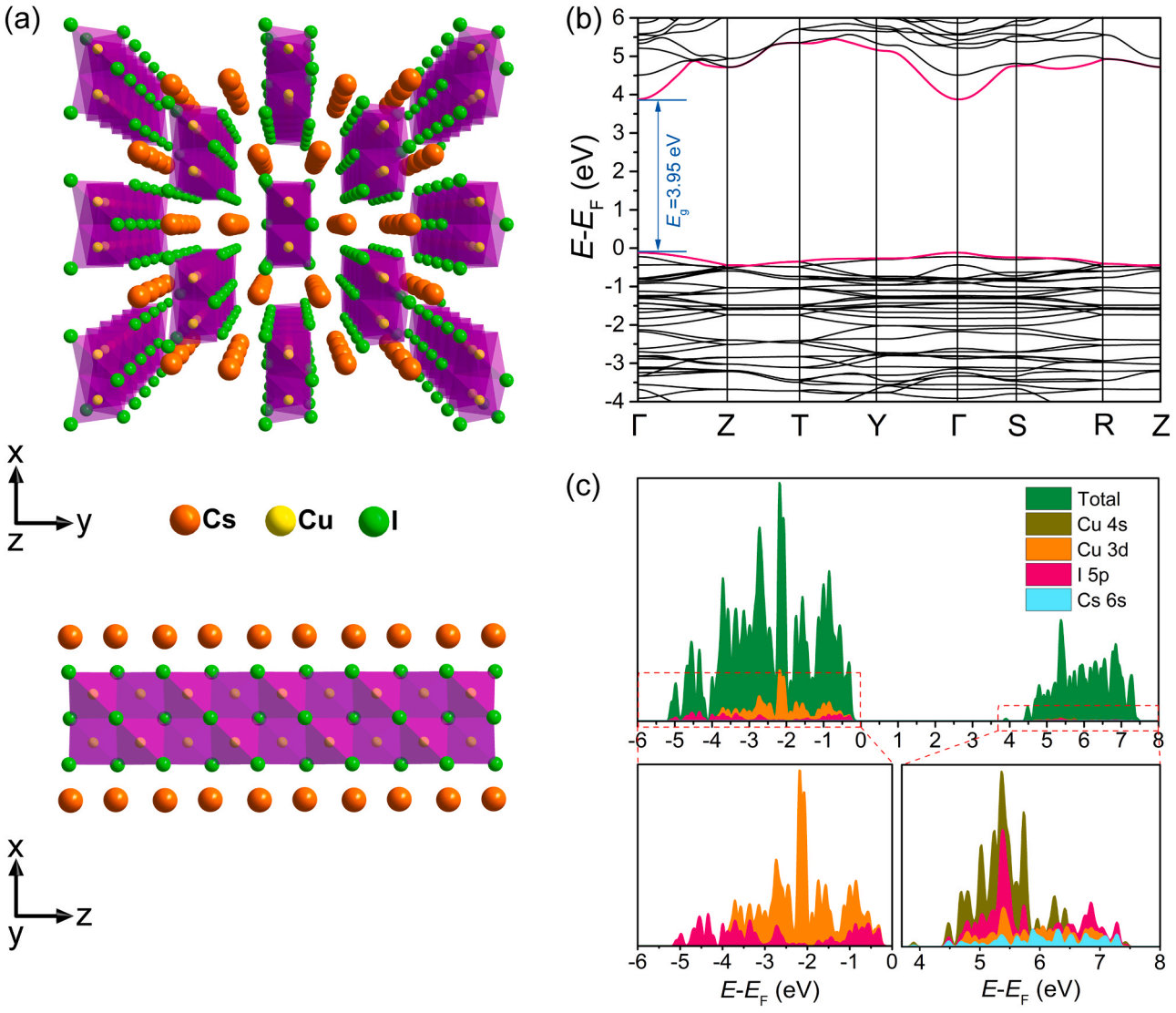

Fig. 1. (a) Crystal structures of 1D $CsCu_2I_3$ projected along the [001] and [010] directions. (b) Calculated electronic band structure of the 1D $CsCu_2I_3$ using hybrid PBE0 functional. (c) Total and partial electronic DOS for the 1D $CsCu_2I_3$ using the hybrid PBE0 functional.

time as low as 50.4 ms (at 340 nm). Related device performance and emission mechanism of the 1D $CsCu_2I_3$ SC are demonstrated and discussed in this work.

2. Results and discussion

Fig. 1a illustrates the crystal structures of the 1D $CsCu_2I_3$ along the [001] and [010] directions, showing that the 1D $CsCu_2I_3$ belongs to the orthorhombic *Cmcm* space group (with unit cell parameters: $a = 10.5479$ Å, $b = 13.1725$ Å, $c = 6.0972$ Å, $\alpha = \beta = \gamma = 90°$) [36]. In this structure, the Cu^+ ions reside in the tetrahedrally coordinated interstice created by the anion sublattice to form $[CuI_4]^{3-}$. The double $[CuI_4]^{3-}$ tetrahedral strings, sitting in the rhombic columnar cages composed of Cs^+ cations, are infinitely stacked with edge sharing to form $[Cu_2I_3]^-$ anionic chains in the $CsCu_2I_3$ 1D crystal structure. This structure is distinctly different from the typical 2D and 3D metal halide perovskites where the crystal is stacked with the corner-sharing octahedral $[PbBr_6]^{4-}$ units or the 0D Cu(I)-based halide ($Cs_3Cu_2I_5$) where the Cu^+ ions occupies both the tetrahedral and trigonal sites [24,41]. Stacking of the double $[CuI_4]^{3-}$ strings in this structure is similar to the 1D $C_4N_2H_{14}PbBr_4$ perovskite where the 1D morphology is based on double edge-shared octahedral $[PbBr_6]^{4-}$ units [9]. It is also noticeable that the $[Cu_2I_3]^-$ chains in the 1D $CsCu_2I_3$ lattice are spatially isolated by the Cs^+ ions to form a quasi core-shell structure, suggesting that the 1D $CsCu_2I_3$ may possess high luminescence efficiency like the core-shell nanowires (NWs). To fully comprehend the electronic properties of the 1D $CsCu_2I_3$ at the atomic level, we have performed a density functional theory (DFT) calculation using the hybrid PBE0 functional. The lead-free Cu(I)-based $CsCu_2I_3$ has a direct bandgap of 3.95 eV between the conduction band minimum (CBM) and valence band maximum (VBM) at Γ point (see Fig. 1b), agreeing with other report (3.93 eV) by the DFT calculation using hybrid PBE0 functional [40]. Note that the calculated bandgap in this work is much larger than those by using the PBE functional (in which the bandgap was calculated as 2.15 or 2.05 eV) [38,39]. In fact, the calculated bandgap from the PBE calculation will show big deviation (underestimation) to the experimental optical bandgap owing to the well-accepted bandgap error. That is why we calculated the bandgap of the $CsCu_2I_3$ by the hybrid PBE0 functional to obtain a much accurate bandgap, rather than the PBE functional. The total and partial density of states (DOS) depicted in Fig. 1c suggest that while the CBM of $CsCu_2I_3$ is mainly dominated by the Cu 4s and I 5p orbitals, the VBM is primarily attributed to the Cu 3d and I 5p orbitals. Since Cs^+ contributes little to the CBM and VBM, the Cs^+ cations may act as quasi-isolating shell for the 1D $[Cu_2I_3]^-$ chains (which are only photoactive in the $CsCu_2I_3$) to give efficient light emissions [24]. The calculated absorption spectrum shows well tendency with the experimental results, confirming the validity of the DFT calculation (see Fig. S1).

The crystal structure and ionic conductivity of the $CsCu_2I_3$ have been well studied and described previously [36,42], but the synthesis of $CsCu_2I_3$ SC and its use in optoelectronic applications have rarely been reported [39]. Herein, we report the demonstration of high-quality centimeter-sized 1D $CsCu_2I_3$ SC with length as long as 13 mm for efficient yellow light-emitting and PD applications. To synthesize high-quality $CsCu_2I_3$ SC, we have developed a modified ITC method by using oleic acid (OA) as additive in DMF to suppress the defects formation during the long period of crystal growth under the temperature of 75 °C (see Fig. 2a). We have not utilized AVC method (used to grow $Cs_3Cu_2I_5$ and $CsCu_2I_3$ SC previously [24,39]) to produce the $CsCu_2I_3$ SC because we have found that only small $CsCu_2I_3$ SCs are randomly obtained by the AVC method, rather than a single large bulk $CsCu_2I_3$ SC with smooth surfaces. It should be noted that OA is a crucial additive to prevent the Cu^+ cations from oxidation due to its reducibility during the solvothermal ITC reaction. As the surfactant ligand, OA can also maintain the diffusion equilibrium of ions to slow the crystallization speed to facilitate high-quality growth of the 1D $CsCu_2I_3$ SC with much less bulk defects. Without OA, the crystallization might be too fast to induce considerable bulk defects and a broadband white-light emission would be observed.

Fig. 2b presents the photograph of the as-grown $CsCu_2I_3$ SC, showing that a perfect bulk $CsCu_2I_3$ SC is successfully synthesized with length as long as 13 mm. While the bulk $CsCu_2I_3$ SC is of high transparency under sunlight, it shines bright yellow light under the illumination of 365 nm UV light (Fig. 2b inset). The phase purity of the $CsCu_2I_3$ SC (ground into fine powders) is examined by powder X-ray diffraction (XRD), clearly demonstrating that the SC belongs to the orthorhombic structure of $CsCu_2I_3$ (PDF#45-0076) (see Fig. 2c). Furthermore, 2θ scan on the

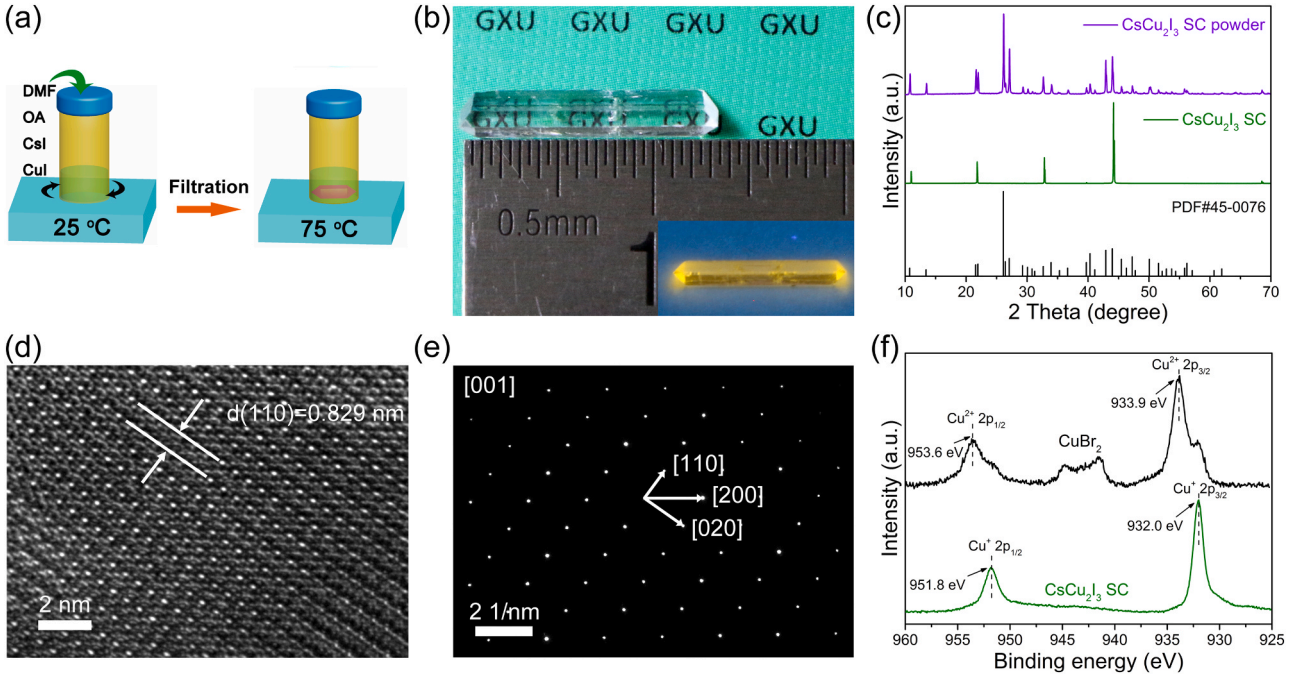

Fig. 2. (a) Scheme for preparation of the 1D $CsCu_2I_3$ SCs via ITC method. (b) Photographs of typical 1D $CsCu_2I_3$ SC under ambient light and 365 nm UV light (inset). Structural and compositional characterizations of the 1D $CsCu_2I_3$ SC: (c) XRD, (d) HRTEM, (e) SAED, and (f) Cu 2p XPS spectra.

maximal facet of the as-grown bulk $CsCu_2I_3$ SC shows five typical sharp peaks at 10.99°, 21.81°, 32.83°, 44.18°, and 68.51°, which correspond to the (110), (220), (330), (440), and (660) planes, respectively (see the green curve in Fig. 2c). All these five XRD peaks match well with the XRD patterns of the $CsCu_2I_3$ SC powder but have ultra-small 2θ FWHM value of merely 0.06–0.09°, indicating the ultra-high quality of $CsCu_2I_3$ SC [43]. Chemical composition profile on different positions of the SC by the energy dispersive X-ray spectroscopy (EDS) verifies the formation of $CsCu_2I_3$ compound (data not shown), agreeing well with the XRD results. High-resolution transmission electron microscope (HRTEM) and selected area electron diffraction (SAED) pattern in Fig. 2d and e firmly demonstrate the single crystallinity of the $CsCu_2I_3$ SC with ultra-high qualities. The *d*-spacing of the adjacent planes is 8.29 Å, which well corresponds to the (110) plane of the $CsCu_2I_3$ compound.

X-ray photoelectron spectroscopy (XPS) measurement is established for the sake of identifying the valency of Cu in the SC, using $CuBr_2$ as the reference (see Fig. 2f). C 1s peak of the adsorptive carbon at 284.5 eV was used to correct the binding energies. For the $CuBr_2$ having cupric cations (Cu^{2+}), two distinct peaks at 953.6 and 933.9 eV (which correspond to the Cu $2p_{1/2}$ and Cu $2p_{3/2}$, respectively) and two satellite peaks at 944.7 and 941.4 eV are observed in the Cu 2p XPS spectrum. This is the typical XPS spectrum for Cu^{2+} that can be found in the handbooks or literatures [37,44,45]. For the $CsCu_2I_3$ SC that has cuprous cations (Cu^{+}), however, it has quite different Cu 2p XPS spectrum as compared with the $CuBr_2$ and only two Cu 2p peaks at 951.8 and 932.0 eV are observed in the XPS spectrum, suggesting that the Cu 2p signals in the SC should not originate from the Cu^{2+} but from the Cu^{+} (agreeing with the XRD results). These results also suggest that OA successfully protects the Cu^{+} from being oxidized to Cu^{2+} even under temperature of 75 °C for long duration reaction (72 h). In fact, it is found that the Cu^{+} is quite safe even under much higher temperature of 120 °C with the protection of OA in our experiment.

Organic-inorganic metal halide perovskites are suffering severe problems on thermal stability because of the fundamentally volatile nature of their organic molecules [46]. All-inorganic halide perovskites and compounds are proved to be more thermally stable in higher temperatures due to the lack of numerous phase transitions [47]. In consideration of this, it is highly important to investigate the thermal stability of the $CsCu_2I_3$ SC. On the basis of thermogravimetric analysis (TGA) measurement, the $CsCu_2I_3$ SC shows negligible mass loss up to 480 °C (see Fig. 3a), demonstrating high thermal stability that are superior over the $CH_3NH_3PbI_3$ and $CsPbI_3$ perovskites [48–51]. The differential scanning calorimetry (DSC) scan shows that the $CsCu_2I_3$ SC undergoes three thermal events at T_1 (383 °C), T_2 (475 °C), and T_3 (525 °C). T_1 peak at 383 °C suggests the incongruent melting behavior of the $CsCu_2I_3$ compound. With increasing heating temperature, the $CsCu_2I_3$ compound will continuously decomposes to CuI and CsI, resulting in two melting transitions at T_2 and T_3. The high decomposition temperature firmly suggests the high thermal stability of the $CsCu_2I_3$ SC, which guarantees its wide applications in variety of optoelectronic devices.

Fig. 3b presents the optical properties of the $CsCu_2I_3$ SC by photoluminescence (PL) and PL excitation (PLE) measurements at RT. As shown in Fig. 3b, the $CsCu_2I_3$ SC emits bright single-band yellow emission at 580 nm under UV excitation, consistent with the shining yellow light in the inset of Fig. 2b. The observed bright yellow emission may stem from the strongly localized excitons because of the strong quantum confinement of low-dimensional core-shell structure of the 1D $CsCu_2I_3$. In comparison with the PL, the PLE spectrum shows a Stokes shift as large as 240 nm into the UV range (340 nm), suggesting that the single-band yellow emission of the $CsCu_2I_3$ SC is ascribed to the self-trapped excitons (see Fig. 3c) [9,24]. It is noted that the optical bandgap derived from the PLE peak (340 nm, or 3.65 eV) is well consistent with the bandgap obtained by the PBE0 calculations (3.95 eV), confirming the accuracy of the DFT calculation in our work. The calculated bandgap is a little higher by 0.3 eV than the PLE energy, possibly because that the exciton bingding is not considered during the calculation [40]. The smaller emission peak at 580 nm (2.14 eV) than the calculated bandgap of 3.95 eV clearly demonstrates the validity of the transition model by the self-trapped excitons shown in Fig. 3c. The absolute PLQY of $CsCu_2I_3$ SC is measured to be as high as 50.4% at RT (see Fig. S2), which is comparable to the best of some of the all-inorganic yellow-emitting lead halide perovskites and much more superior than the reported Cu (I)-based $CsCu_2I_3$ halides (see Table 1). The PL intensity of the $CsCu_2I_3$ SC remains nearly unchanged after storage for over 2,200 h in ambient air (RH: 40%), indicative of the ultra-high stability of the $CsCu_2I_3$ SC in air (see Fig. 3d). These results suggest that the Cu^{+} is ultra-stable in the unique 1D $CsCu_2I_3$ crystal structure. In fact, the high air-stability

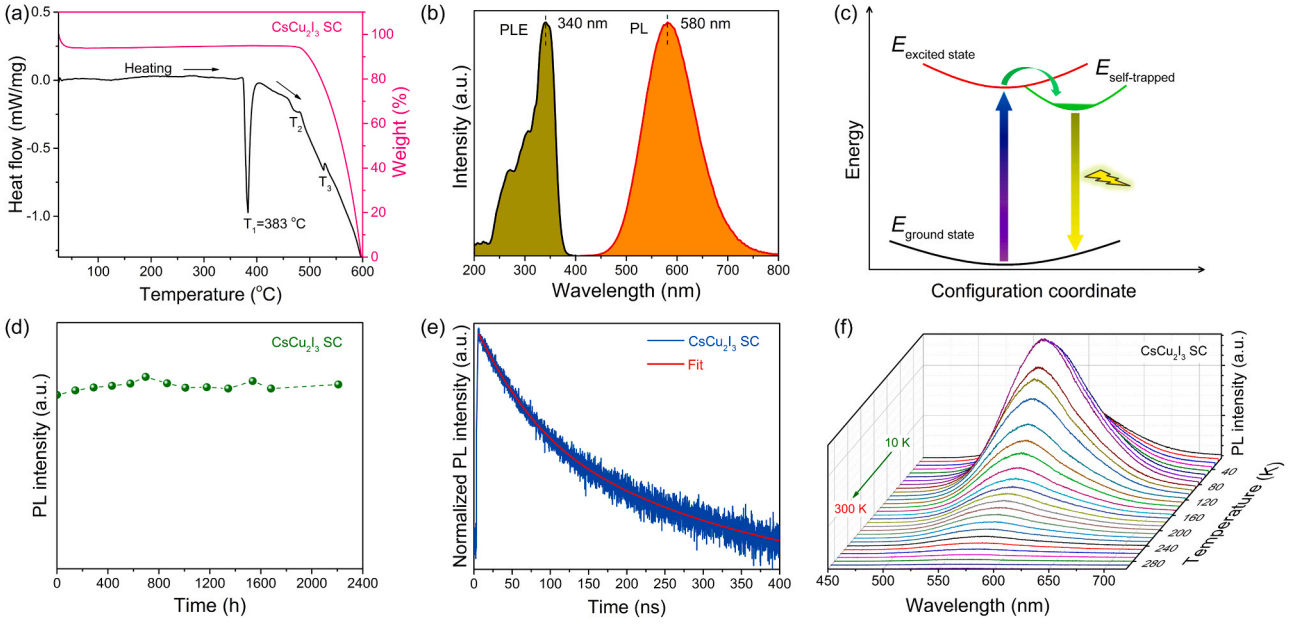

Fig. 3. Thermal and optical properties of the 1D $CsCu_2I_3$ SC: (a) TGA (pink line) and DSC (black line) plots showing high thermal stability; (b) PLE and PL spectra; (c) Configuration coordinate diagram for the photophysical process of the yellow emissions in the 1D $CsCu_2I_3$ SC. (d) PL stability versus different storage time in ambient air with RH of 40%; (e) TRPL decay. (f) TDPL spectra from 10 to 300 K.

Table 1
Summarization of PLQYs for all-inorganic yellow-light-emitting lead halide perovskites and lead-free 1D $CsCu_2I_3$ halide compounds.

Materials	Morphology	Dimension	Emission peak (nm)	PLQY (%)	Ref.
$CsPbBr_{1.5}I_{1.5}$	Nanocrystal	3D	579	50	[62]
$CsPb_{0.73}Mn_{0.27}Cl_3$	Quantum dot	3D	579	54	[63]
$CsPb_{0.94}Mn_{0.06}Cl_3$	Quantum dot	3D	574	22	[63]
$CsPbBr_{1.3}I_{1.7}$	Nanocrystal	3D	556	40	[64]
$CsCu_2I_3$	Nanorod	1D	561	11	[26]
$CsCu_2I_3$	SC	1D	~583	6.5	[29]
$CsCu_2I_3$	Nanowire	1D	542	–	[30]
$CsCu_2I_3$	Thin film	1D	548	20.6	[32]
$CsCu_2I_3$	Powder crystal	1D	558	–	[34]
$CsCu_2I_3$	Nanocrystal	1D	553	5.0	[38]
$CsCu_2I_3$	SC	1D	568	15.7	[39]
$CsCu_2I_3$	Powder	1D	576	3.23	[40]
$CsCu_2I_3$	SC	1D	580	50.4	This work

property of the Cu^+-based halides was also observed previously in other Cu(I)-based halides, possibly owing to the robust chemical bonds between the Cu^+ and halogen ions in such a unique 1D crystal structure [38,40]. Fig. 3e shows the time-revolved PL (TRPL) of the $CsCu_2I_3$ SC, in which the decay profile can be obtained by the two-exponential function fitting:

$$I(t) = A_1 e^{(-t/\tau_1)} + A_2 e^{(-t/\tau_2)} + I_0 \quad (1)$$

where the fast component τ_1 and the slow component τ_2 can be obtained as 43 and 182 ns, respectively, resulting in an average exciton lifetime of τ_{ave} ~135 ns. This lifetime is much shorter than that of 0D $Cs_3Cu_2I_5$ SC (~464 ns) [24], but is close to 1D $C_4N_2H_{14}PbBr_4$ perovskite bulk crystals, suggesting that the $CsCu_2I_3$ SC may have the similar PL mechanism as that of the 1D perovskite $C_4N_2H_{14}PbBr_4$ from self-trapped excitons [9]. The fast decay τ_1 is attributed to traps-assisted recombination of photo-excited electrons and holes at the $CsCu_2I_3$ SC surface, while the slow decay τ_2 is usually thought to be related to the recombination inside the $CsCu_2I_3$ SC [43].

Temperature-dependent PL (TDPL) (10–300 K) was measured to investigate the dynamics of the self-trapped excitons (see Fig. 3f). It is seen that only one emission peak is observed as the temperature is increased, indicating that the yellow emission results from the $CsCu_2I_3$ SC, rather than other impurities. For detail investigation on the PL intensity at each temperature, one can find that the PL intensity firstly increases from 10 to 80 K (see Fig. S3), but then decreases with further improving the temperature from 80 to 300 K (see Fig. 3f). This interesting phenomenon is completely different from previously reported Cu (I)-based halides whose PL intensity monotonously decreases with increasing the temperature owing to the greatly enhanced trapping of charge carriers at higher temperatures [24,39,40]. Previously, S. Hull et al. suggested that $CsCu_2I_3$ exhibited relatively large anisotropic thermal vibrations and might undergo a phase transition from *Cmcm* to *Pbnm* symmetry at low temperature [36]. However, on the basis of the TDPL results, the peak position of the PL remains nearly unchanged within the temperature range from 10 to 80 K (see Fig. S3), and thereby the effects of phase transitions at low temperature suggested by S. Hull et al. can be ruled out. In fact, similar negative thermal quenching phenomenon was also observed in the Mn^{2+}- and Cd^{2+}-doped $CsPbCl_3$ nanocrystals, in which shallow metastable states that lay close to the excitonic states were thought to be responsible for this phenomenon [52,53]. Charge carriers trapped in the shallow metastable states can return to the excitonic states ($E_{excited\ state}$ in Fig. 3c) at moderate temperature (80 K in our case) and as a result, more charge carriers are transferred to the self-trapped states to recombine radiatively. Hence, with increasing temperature from 10 to 80 K, more charge carriers trapped in the shallow metastable states may have sufficient thermal energy to repopulate the charge carriers to $E_{excited\ state}$, thus resulting in enhanced PL intensity from 10 to 80 K. Higher than the temperature of 80 K, however, the thermally trapping population of charge carriers are greatly enhanced so that the carriers trapped are much more than those returned from the shallow metastable states, thus leading to progressive decrease of the PL intensity from 80 to 300 K.

The superior PLQY of the $CsCu_2I_3$ SC and outstanding thermal air stability make it great potential as yellow phosphors to produce WLEDs. To fabricate WLEDs, we blended ultra-fine powders of the $CsCu_2I_3$ SC with commercial blue phosphors ($BaMgAl_{10}O_{17}:Eu^{2+}$) together in silicone resin as the composite phosphors of 365 nm UV LED chips. Fig. 4a shows the typical EL emission spectra of the WLEDs with increasing forward-biasing voltages. In comparison with the I–V curves and EL spectra of pure blue and yellow LEDs using pure $BaMgAl_{10}O_{17}:Eu^{2+}$ and $CsCu_2I_3$ SC phosphors individually (see Fig. S4), we verify that the distinct blue and yellow bands in the EL of the WLED result from $BaMgAl_{10}O_{17}:Eu^{2+}$ and $CsCu_2I_3$ SC, respectively. It is also noted that the spectral shape of the WLED nearly remains the same with the increase of forward-biasing voltages, indicating the extraordinary stability and great potential applications of the $CsCu_2I_3$ SC as yellow phosphors in WLEDs. The CIE 1931 chromaticity coordinate and correlated color temperature (CCT) of the WLED are determined to be (0.27, 0.31) and 10,000 K (Fig. 4b), respectively, belonging to a cold white-light source (see Fig. 4d). The WLED delivers good color rendering for colorful objects (see Fig. 4b inset). Most strikingly, the WLED is capable of working at a continuous driving current of 50 mA for more than 580 h in ambient air with RH of 40% (see Fig. 4c), demonstrating the ultra-high stability of the $CsCu_2I_3$ SC. The half-lifetime of the WLED is estimated to be L_{50} ≈ 150 h, comparable to the LEDs using all-inorganic $CsPbX_3$ perovskites or double perovskites as phosphors [21,54].

PDs having a planar metal-semiconductor-metal (MSM) architecture of Ni/$CsCu_2I_3$ SC/Ni were designed and fabricated to further develop the optoelectronic applications of the $CsCu_2I_3$ SCs (see Fig. 5b left inset). Prior to evaluate the performance of the PDs, trap density (n_{trap}) and carrier mobility (μ) of the $CsCu_2I_3$ SC were estimated from the dark I–V characteristics of a Ni-sandwiched $CsCu_2I_3$ SC hole-only device in which Ni electrodes (8.75 mm^2) were deposited on both parallel sides of the $CsCu_2I_3$ SC by sputtering (see Fig. 5a inset). As shown in Fig. 5a, three regions can be obtained from the dark I–V curve with the log-log scale: the Ohmic region ($I \propto V^{n=1}$, $V < 46.7$ V); the Child's region ($I \propto V^{n=2}$, $V > 80.7$ V); the trap filled limit (TFL) region ($46.7 < V < 80.7$ V). The applied voltage at the kink point between the Ohmic and TFL region is also called TFL voltage (V_{TFL}) and can be determined by the n_{trap} as:

$$V_{TFL} = \frac{e n_{trap} t^2}{2\varepsilon\varepsilon_0} \quad (2)$$

where e is the elementary charge, t is the thickness of the $CsCu_2I_3$ SC, ε is the relative dielectric constant of the $CsCu_2I_3$ SC, and ε_0 is the vacuum permittivity. The relative dielectric constant ε can be calculated to be 28.6 by measuring the capacitance of the Ni-sandwiched $CsCu_2I_3$ SC device with a Tonghui TH2828 precision LCR meter and using the equation $\varepsilon = Ct/\varepsilon_0 A$, where A is the area of the Ni electrodes. As a result, the trap density of the $CsCu_2I_3$ SC is determined to be 2.95×10^{10} cm^{-3}, which is comparable with those of the best perovskite SCs and indicates the high quality of the $CsCu_2I_3$ SC [55,56]. At higher bias in the Child's region, a space charge-limited current (SCLC) model can be established, and the dark current was determined by the Mott-Gurney law [55]:

$$J_D = \frac{9\varepsilon\varepsilon_0 \mu V_b^2}{8t^3} \quad (3)$$

where J_D is the dark current density, and V_b is the applied voltage. The carrier mobility μ is calculated to be 18.61 cm^2 V^{-1} s^{-1}, comparable

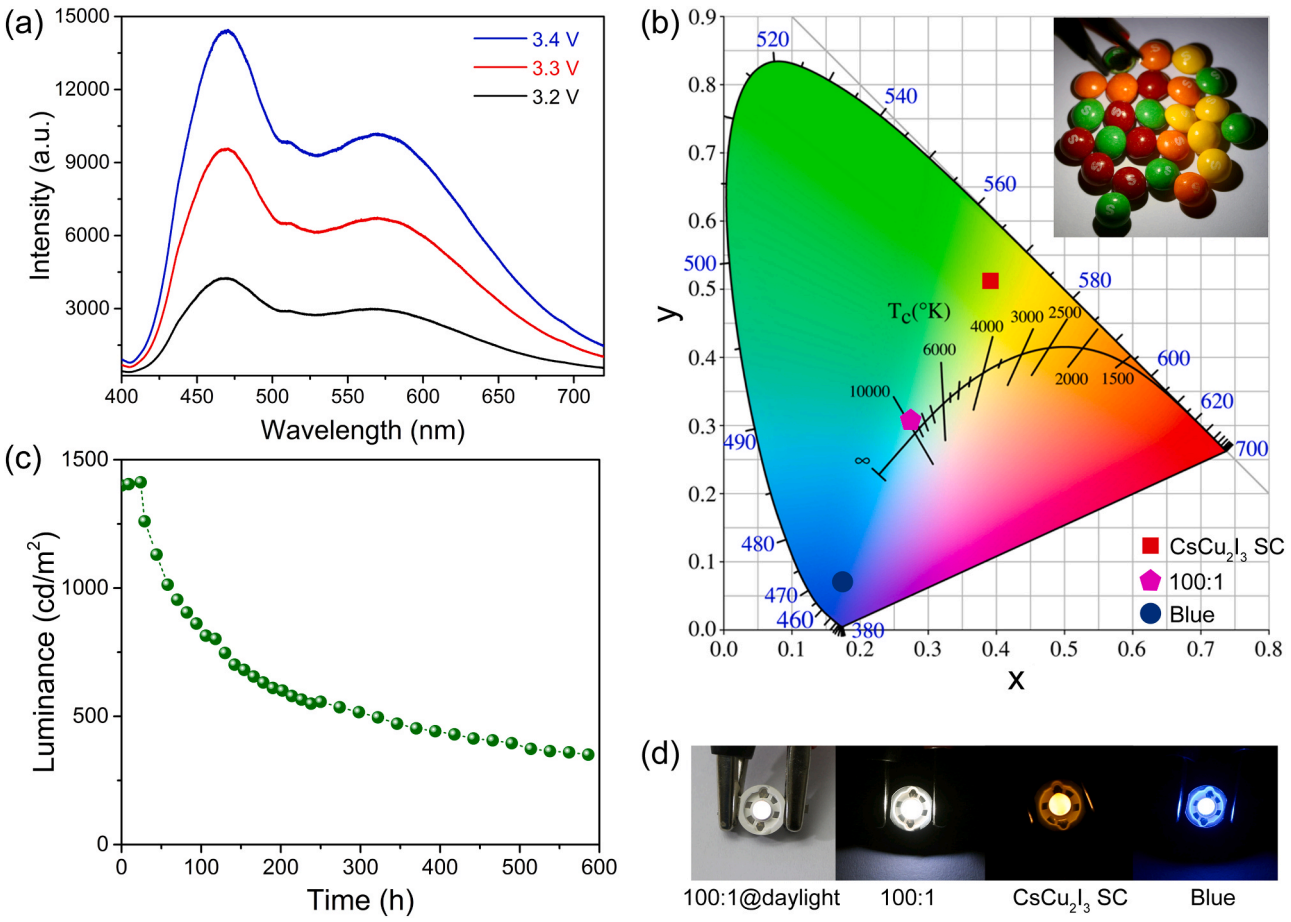

Fig. 4. (a) EL spectra of the WLED with increasing driving voltages. (b) CIE coordinates of the blue, yellow and white LEDs. The inset shows the photograph of candies illuminated by the WLED. (c) Lifetime measurement of the WLED at continuous driving current of 50 mA in air atmosphere. (d) Photographs of the LEDs with lighting up at driving current of 50 mA, showing bright blue-, yellow-, and white-light emissions. For the WLEDs, the weight ratio of the yellow to blue phosphors is used as 100: 1. (For interpretation of the references to colour in this figure legend, the reader is referred to the web version of this article.)

with the perovskite SCs and much larger than the $Cs_3Cu_2I_5$ halide [27]. Both the low trap density and high carrier mobility indicate that the $CsCu_2I_3$ SC is of high-quality and suitable for fabricating PDs.

Fig. 5b illustrates the spectral response of the Ni/$CsCu_2I_3$ SC/Ni MSM PD under bias voltage of − 5 V. The PD shows narrow-band spectral response in the UV range at 365 nm, which agrees with the PLE peak (340 nm) except for a negligible deviation of 25 nm. The UV response at 365 nm verifies validity of the transition model supposed in Fig. 3c and indicates that the bright yellow light of the $CsCu_2I_3$ SC comes from the self-trapped excitons. The deviation as well as the observation of a shoulder peak near 330 nm in the response spectra might be attributed to the self-absorption and multiple light reflections among the internal surfaces of the $CsCu_2I_3$ SC [57]. For the purpose of consistency with the PLE results, we used 340 nm UV light as the source (3.29 mW/cm^2) to investigate the performance of the PD. As seen in the Fig. 5b right inset, the device presents distinct photoresponse under illumination of the 340 nm UV light, as compared with the dark case. The asymmetric feature of the I–V curve under forward and reverse bias might be ascribed to the negligible difference of the Schottky contacts between the Ni electrodes and the $CsCu_2I_3$ SC formed during sputtering. Fig. 5c shows the time-dependent photocurrent response of the UV PD. From the plot, one can see that the UV PD can work stably with high reproducibility even after multiple operation circles. A current ON/OFF ratio of 3.7 is obtained from the device even with such a high electrode distance of 3 mm, owing to the high crystal quality of the $CsCu_2I_3$ SC by reducing the grain-boundary recombination of the carriers [43]. The ON/OFF ratio shall be much higher if interdigital electrodes with much smaller electrode distance were used, as that in the reported literature [30]. The rise time (t_r) and fall time (t_f) were measured to be 50.4 and 244.8 ms (Fig. 5d), respectively, which are comparable with those UV PDs using perovskite SCs and much more superior than those of Ga_2O_3- and ZnO-based UV PDs (see Table S1). We attribute the fast response of the PD to the high quality of the 1D $CsCu_2I_3$ SC.

3. Experimental section

3.1. Materials synthesis and device fabrication

3.1.1. Chemicals and reagents

Cesium iodide (CsI, 99.999%), cuprous iodide (CuI, 99.95%), and oleic acid (OA, 85%) were bought from Aladdin Corporation. Anhydrous N,N-dimethylformamide (DMF, 99.5%) was purchased from Sinopharm Chemical Reagent Co. Ltd. (China). All the raw materials and solvents were used as received without further purification unless stated elsewhere.

3.1.2. Synthesis of $CsCu_2I_3$ SCs

The $CsCu_2I_3$ SCs were grown by a modified ITC method [58]. Specifically, CsI (1.2995 g) and CuI (1.9045 g) with a molar ratio of 1:2 were completely dissolved in OA/DMF (0.8 mL/5 mL) mixed solvent under vigorously stirring for 30 min in ambient environment at RT. The resultant greenish solution was then filtered into a glass vial via a poly (tetrafluoroethylene) (PTFE) filter (0.22 μm) to remove the undesirably undissolved precursors or contaminations. The glass vial was quickly

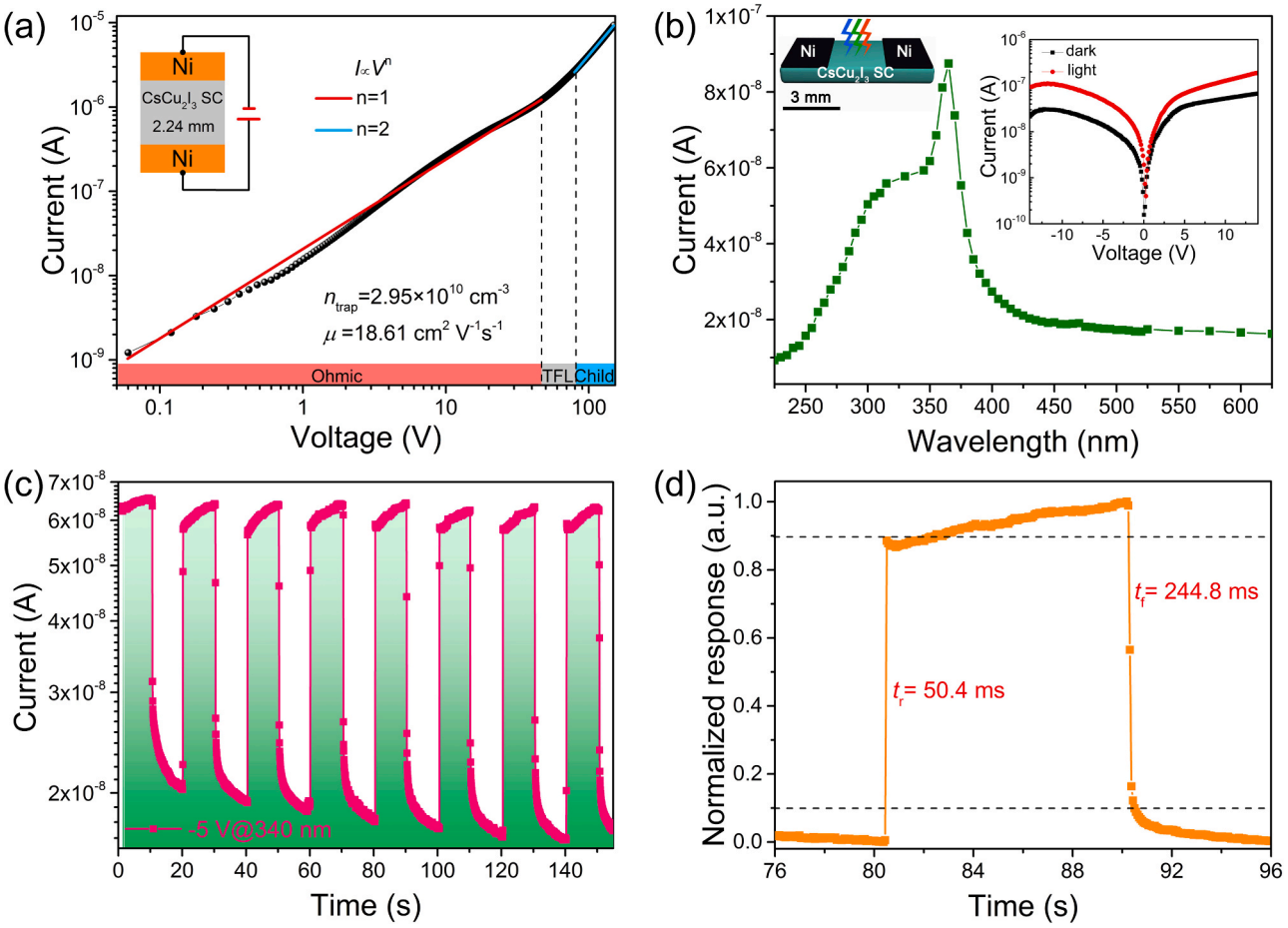

Fig. 5. (a) I–V curve to derive the trap density and carrier mobility of the 1D $CsCu_2I_3$ SC. (b) Spectral response of the Ni/1D $CsCu_2I_3$ SC/Ni MSM PD under bias voltage of − 5 V. The insets illustrate the device structure and the I–V curves with and without illumination of 340 nm UV light. (c) Periodic photocurrent response of the PD. (d) Rising and falling edges of the PD to estimate the rise time (t_r) and fall time (t_f).

sealed with its cover and placed in an oil bath (see Fig. 2a). The solution in the glass vial shall gradually turn into dark brown with increasing temperature of the oil bath. The temperature was elevated with a suitable heating rate of 2 °C/h (a vitally optimized parameter) until the dark-brown solution crystallized one or two small $CsCu_2I_3$ seeds in the vial (75 °C). Afterward, the elevation procedure of the temperature was immediately ceased with the temperature maintaining at 75 °C to facilitate the continuous growth of the $CsCu_2I_3$ seeds to finally become a 13 mm $CsCu_2I_3$ SC for 72 h. All the procedures were conducted under ambient air conditions with the RH controlled to be 40–50%.

3.1.3. Preparation of UV pumped WLEDs

$CsCu_2I_3$ SCs were ground into ultrafine powders as the yellow-light phosphors, and commercially purchased blue $BaMgAl_{10}O_{17}:Eu^{2+}$ phosphors were used as the blue-light emitter. For preparing WLEDs, the blended yellow and blue phosphors (with weight ratio of 100:1) were mixed thoroughly with a thermally curable silicone resin by a weight ratio of 0.8:1 as the light emitter of 365 nm UV LED chips. After adding the hardener, the resultant composite paste was covered onto the UV LED chips. Finally, the LED chip was dried at 100 °C for 40 min to solidify the phosphors/silicone resin to produce the WLEDs. For preparing pure yellow (blue) LEDs, the procedures were similar but only yellow $CsCu_2I_3$ SC (blue $BaMgAl_{10}O_{17}:Eu^{2+}$) powders were used as the phosphors.

3.1.4. Preparation of Ni/$CsCu_2I_3$ SC/Ni PDs

For preparing planar MSM PDs, nickel (Ni, ~250 nm) was sputtered on the $CsCu_2I_3$ SC directly as electrodes by using a shadow mask. The distance of the two Ni electrodes was controlled to be 3 mm. For performance investigation, a Xenon lamp coupled with a Zolix monochromator was used as the light source. The obtained Ni/$CsCu_2I_3$ SC/Ni PDs were covered with black mask except for the active illumination area between the two Ni electrodes during the performance test. A Keithley 2400 sourcemeter was used to measure the I–V traces of the PDs. Light power at each wavelength was measured with a Thorlabs PM100D optical power and energy meter that was attached with a calibrated Si photodiode.

3.1.5. DFT calculations

Electronic properties of the $CsCu_2I_3$ were performed by first-principles (FP) calculations with the VASP code using projector augmented wave (PAW) method [59–61]. The exchange and correlation potentials were treated with Perdew–Burke–Ernzerhof (PBE) generalized gradient approximation (GGA). Instead of PBE functional, we calculated the electronic band structure, density of states (DOS), and absorption spectrum of the $CsCu_2I_3$ by hybrid PBE0 functional. Convergence of the FP calculations was ensured by setting the plane-wave energy cutoff to 500 eV. The mesh samplings in the Brillöuin zone (BZ) were 11 × 11 × 15.

3.2. Characterization methods

Structural properties of the $CsCu_2I_3$ SCs was investigated by XRD (Rigaku MiniFlex600, Cu Kα radiation). EDS was characterized by Oxford Instruments X-Max^N system equipped in JEOL JXA-8230 electron probe microanalyzer (EPMA). TEM, HRTEM and SAED measurements

were performed in FEI Tecnai G2 F20 S-TWIN. XPS was measured by ESCALAB 250Xi (Thermo Scientific). TGA and DSC results were obtained using TGA/DSC-2 (Mettler Toledo), heating at a steady rate of 10 °C/min under a 20 mL/min Ar flow. Absorption spectra were tested by a PerkinElmer Lambda950 UV–Vis spectrophotometer. PL, PLE and absolute PLQY of the $CsCu_2I_3$ SC were measured by Edinburgh FLS980 spectrometer equipped with a Xenon lamp source and an integrating sphere. Temperature-dependent PL was tested using a low-temperature system (Janis CCS-150) and a CCD-equipped spectrometer (Acton SP2500i). TRPL was measured in a Zolix-750 system excited by a 375 nm picosecond pulsed laser (44 ps, 10 MHz, and 10 mW). Time-dependent PL stability was studied by excitation of a He–Cd laser (325 nm, IK3201R-F, Kimmon Koha) and recorded by an Andor iDus CCD detector. EL spectra of the LEDs were measured by the same Andor CCD. I–V curves of the LEDs and PDs were obtained by a home-made I–V measurement system centered with a Keithley 2400 sourcemeter. Luminance of the LEDs was recorded by a KONICA MINOLTA Luminance Meter (LS-150). Canon EOS 70D was used to take all the photographs in this work.

4. Conclusion

In summary, we have synthesized all-inorganic lead-free Cu(I)-based 1D $CsCu_2I_3$ SC by using ITC method. The 1D $CsCu_2I_3$ SC exhibits ultra-high quality with length as long as 13 mm and emits bright yellow light with a champion PLQY as high as 50.4%. Thermal analysis demonstrates that the 1D $CsCu_2I_3$ SC shows high thermal stability even up to 480 °C, which is much more superior than the organic-inorganic metal halide perovskites. Furthermore, the 1D $CsCu_2I_3$ SC also presents ultra-high PL stability in ambient air for over 2,200 h. TRPL results prove that the 1D $CsCu_2I_3$ SC has an average exciton lifetime of ~68 ns. WLEDs produced by using the bright yellow emitting 1D $CsCu_2I_3$ SC as yellow phosphors of UV LEDs are capable of working at a continuous driving current of 50 mA for more than 580 h in ambient air with a half-lifetime of ~150 h. PDs fabricated by the 1D $CsCu_2I_3$ SC shows distinct UV response at 365 nm with fast response time as low as 50.4 ms (at 340 nm). Our results pave a way by using the lead-free Cu(I)-based 1D $CsCu_2I_3$ SC for future solid-state lighting and UV photodetection applications.

CRediT authorship contribution statement

Xiaoming Mo: Conceptualization, Methodology, Writing-original draft, Writing-review and editing. **Tao Li:** Methodology, Investigation, Writing - review & editing. **Fengchang Huang:** Writing - review & editing. **Zhuxin Li:** Methodology, Validation. **Yulu Zhou:** Writing - review & editing. **Tao Lin:** Methodology. **Yifang Ouyang:** Software. **Xiaoma Tao:** Simulation, Resources, Supervision. **Caofeng Pan:** Conceptualization, Resources, Supervision, Writing - review & editing, Validation.

Declaration of Competing Interest

The authors declare that they have no known competing financial interests or personal relationships that could have appeared to influence the work reported in this paper.

Acknowledgements

This work was financially supported by National Natural Science Foundation of China (Grant No. 11504060, 11865004), and Natural Science Foundation of Guangxi Zhuang Autonomous Region, China (Grant No. 2018GXNSFBA281163).

Appendix A. Supporting information

Supplementary data associated with this article can be found in the online version at doi:10.1016/j.nanoen.2020.105570.

References

[1] M.A. Green, A. Ho-Baillie, H.J. Snaith, The emergence of perovskite solar cells, Nat. Photonics 8 (2014) 506–514, https://doi.org/10.1038/nphoton.2014.134.
[2] L.N. Quan, B.P. Rand, R.H. Friend, S.G. Mhaisalkar, T.W. Lee, E.H. Sargent, Perovskites for next-generation optical sources, Chem. Rev. 119 (2019) 7444–7477, https://doi.org/10.1021/acs.chemrev.9b00107.
[3] H. Min, M. Kim, S.U. Lee, H. Kim, G. Kim, K. Choi, J.H. Lee, S.I. Seok, Efficient, stable solar cells by using inherent bandgap of α-phase formamidinium lead iodide, Science 366 (2019) 749–753, https://doi.org/10.1126/science.aay7044.
[4] K. Lin, J. Xing, L.N. Quan, F.P.G. de Arquer, X. Gong, J. Lu, L. Xie, W. Zhao, D. Zhang, C. Yan, W. Li, X. Liu, Y. Lu, J. Kirman, E.H. Sargent, Q. Xiong, Z. Wei, Perovskite light-emitting diodes with external quantum efficiency exceeding 20 per cent, Nature 562 (2018) 245–248, https://doi.org/10.1038/s41586-018-0575-3.
[5] G. Xing, N. Mathews, S.S. Lim, N. Yantara, X. Liu, D. Sabba, M. Grätzel, S. Mhaisalkar, T.C. Sum, Low-temperature solution-processed wavelength-tunable perovskites for lasing, Nat. Mater. 13 (2014) 476–480, https://doi.org/10.1038/nmat3911.
[6] Y. Liu, X. Ren, J. Zhang, Z. Yang, D. Yang, F. Yu, J. Sun, C. Zhao, Z. Yao, B. Wang, Q. Wei, F. Xiao, H. Fan, H. Deng, S. (F.) Liu, 120 mm single-crystalline perovskite and wafers: towards viable applications, Sci. China Chem. 60 (2017) 1367–1376, https://doi.org/10.1007/s11426-017-9081-3.
[7] M. Yuan, L.N. Quan, R. Comin, G. Walters, R. Sabatini, O. Voznyy, S. Hoogland, Y. Zhao, E.M. Beauregard, P. Kanjanaboos, Z. Lu, D.H. Kim, E.H. Sargent, Perovskite energy funnels for efficient light-emitting diodes, Nat. Nanotechnol. 11 (2016) 872–877, https://doi.org/10.1038/nnano.2016.110.
[8] Y. Cao, N. Wang, H. Tian, J. Guo, Y. Wei, H. Chen, Y. Miao, W. Zou, K. Pan, Y. He, H. Cao, Y. Ke, M. Xu, Y. Wang, M. Yang, K. Du, Z. Fu, D. Kong, D. Dai, Y. Jin, G. Li, H. Li, Q. Peng, J. Wang, W. Huang, Perovskite light-emitting diodes based on spontaneously formed submicrometre-scale structures, Nature 562 (2018) 249–253, https://doi.org/10.1038/s41586-018-0576-2.
[9] Z. Yuan, C. Zhou, Y. Tian, Y. Shu, J. Messier, J.C. Wang, L.J. Van De Burgt, K. Kountouriotis, Y. Xin, E. Holt, K. Schanze, R. Clark, T. Siegrist, B. Ma, One-dimensional organic lead halide perovskites with efficient bluish white-light emission, Nat. Commun. 8 (2017) 14051, https://doi.org/10.1038/ncomms14051.
[10] M.I. Saidaminov, J. Almutlaq, S. Sarmah, I. Dursun, A.A. Zhumekenov, R. Begum, J. Pan, N. Cho, O.F. Mohammed, O.M. Bakr, Pure Cs_4PbBr_6: highly luminescent zero-dimensional perovskite solids, ACS Energy Lett. 1 (2016) 840–845, https://doi.org/10.1021/acsenergylett.6b00396.
[11] Y. Zhang, M.I. Saidaminov, I. Dursun, H. Yang, B. Murali, E. Alarousu, E. Yengel, B. A. Alshankiti, O.M. Bakr, O.F. Mohammed, Zero-dimensional Cs_4PbBr_6 perovskite nanocrystals, J. Phys. Chem. Lett. 8 (2017) 961–965, https://doi.org/10.1021/acs.jpclett.7b00105.
[12] L. Protesescu, S. Yakunin, M.I. Bodnarchuk, F. Krieg, R. Caputo, C.H. Hendon, R. X. Yang, A. Walsh, M.V. Kovalenko, Nanocrystals of cesium lead halide perovskites (CsPbX3, X = Cl, Br, and I): novel optoelectronic materials showing bright emission with wide color gamut, Nano Lett. 15 (2015) 3692–3696, https://doi.org/10.1021/nl5048779.
[13] J. Song, J. Li, X. Li, L. Xu, Y. Dong, H. Zeng, Quantum dot light-emitting diodes based on inorganic perovskite cesium lead halides ($CsPbX_3$), Adv. Mater. 27 (2015) 7162–7167, https://doi.org/10.1002/adma.201502567.
[14] Z. Shi, Y. Li, Y. Zhang, Y. Chen, X. Li, D. Wu, T. Xu, C. Shan, G. Du, High-efficiency and air-stable perovskite quantum dots light-emitting diodes with an all-inorganic heterostructure, Nano Lett. 17 (2017) 313–321, https://doi.org/10.1021/acs.nanolett.6b04116.
[15] R. Kour, S. Arya, S. Verma, J. Gupta, P. Bandhoria, V. Bharti, R. Datt, V. Gupta, Potential substitutes for replacement of lead in perovskite solar cells: a review, Glob. Chall. 3 (2019), 1900050, https://doi.org/10.1002/gch2.201900050.
[16] M. Lyu, J.H. Yun, P. Chen, M. Hao, L. Wang, Addressing toxicity of lead: progress and applications of low-toxic metal halide perovskites and their derivatives, Adv. Energy Mater. 7 (2017), 1602512, https://doi.org/10.1002/aenm.201602512.
[17] M.R. Filip, S. Hillman, A.A. Haghighirad, H.J. Snaith, F. Giustino, Band gaps of the lead-free halide double perovskites $Cs_2BiAgCl_6$ and $Cs_2BiAgBr_6$ from theory and experiment, J. Phys. Chem. Lett. 7 (2016) 2579–2585, https://doi.org/10.1021/acs.jpclett.6b01041.
[18] E.T. McClure, M.R. Ball, W. Windl, P.M. Woodward, Cs_2AgBiX_6 (X = Br, Cl): new visible light absorbing, lead-free halide perovskite semiconductors, Chem. Mater. 28 (2016) 1348–1354, https://doi.org/10.1021/acs.chemmater.5b04231.
[19] G. Volonakis, M.R. Filip, A.A. Haghighirad, N. Sakai, B. Wenger, H.J. Snaith, F. Giustino, Lead-free halide double perovskites via heterovalent substitution of noble metals, J. Phys. Chem. Lett. 7 (2016) 1254–1259, https://doi.org/10.1021/acs.jpclett.6b00376.
[20] G. Volonakis, A.A. Haghighirad, R.L. Milot, W.H. Sio, M.R. Filip, B. Wenger, M. B. Johnston, L.M. Herz, H.J. Snaith, F. Giustino, $Cs_2InAgCl_6$: a new lead-free halide double perovskite with direct band gap, J. Phys. Chem. Lett. 8 (2017) 772–778, https://doi.org/10.1021/acs.jpclett.6b02682.
[21] J. Luo, X. Wang, S. Li, J. Liu, Y. Guo, G. Niu, L. Yao, Y. Fu, L. Gao, Q. Dong, C. Zhao, M. Leng, F. Ma, W. Liang, L. Wang, S. Jin, J. Han, L. Zhang, J. Etheridge, J. Wang, Y. Yan, E.H. Sargent, J. Tang, Efficient and stable emission of warm-white light

from lead-free halide double perovskites, Nature 563 (2018) 541–545, https://doi.org/10.1038/s41586-018-0691-0.
[22] P. Han, X. Zhang, X. Mao, B. Yang, S. Yang, Z. Feng, D. Wei, W. Deng, T. Pullerits, K. Han, Size effect of lead-free halide double perovskite on luminescence property, Sci. China Chem. 62 (2019) 1405–1413, https://doi.org/10.1007/s11426-019-9520-1.
[23] Z. Xiao, K. Du, W. Meng, D.B. Mitzi, Y. Yan, Chemical origin of the stability difference between copper(I)- and silver(I)-based halide double perovskites, Angew. Chem. Int. Ed. 56 (2017) 12107–12111, https://doi.org/10.1002/anie.201705113.
[24] T. Jun, K. Sim, S. Iimura, M. Sasase, H. Kamioka, J. Kim, H. Hosono, Lead-free highly efficient blue-emitting $Cs_3Cu_2I_5$ with 0D electronic structure, Adv. Mater. 30 (2018), 1804547, https://doi.org/10.1002/adma.201804547.
[25] R. Roccanova, A. Yangui, H. Nhalil, H. Shi, M.-H. Du, B. Saparov, Near-unity photoluminescence quantum yield in blue-emitting $Cs_3Cu_2Br_5$–xIx ($0 \leq x \leq 5$), ACS Appl. Electron. Mater. 1 (2019) 269–274, https://doi.org/10.1021/acsaelm.9b00015.
[26] P. Vashishtha, G.V. Nutan, B.E. Griffith, Y. Fang, D. Giovanni, M. Jagadeeswararao, T.C. Sum, N. Mathews, S.G. Mhaisalkar, J.V. Hanna, T. White, Cesium copper iodide tailored nanoplates and nanorods for blue, yellow, and white emission, Chem. Mater. 31 (2019) 9003–9011, https://doi.org/10.1021/acs.chemmater.9b03250.
[27] Z.-X. Zhang, C. Li, Y. Lu, X.-W. Tong, F.-X. Liang, X.-Y. Zhao, D. Wu, C. Xie, L.-B. Luo, Sensitive deep ultraviolet photodetector and image sensor composed of inorganic lead-free $Cs_3Cu_2I_5$ perovskite with wide bandgap, J. Phys. Chem. Lett. 10 (2019) 5343–5350, https://doi.org/10.1021/acs.jpclett.9b02390.
[28] Y. Li, Z. Shi, W. Liang, L. Wang, S. Li, F. Zhang, Z. Ma, Y. Wang, Y. Tian, D. Wu, X. Li, Y. Zhang, C. Shan, X. Fang, Highly stable and spectrum-selective ultraviolet photodetectors based on lead-free copper-based perovskites, Mater. Horiz. 7 (2020) 530–540, https://doi.org/10.1039/C9MH01371G.
[29] Q. Li, Z. Chen, B. Yang, L. Tan, B. Xu, J. Han, Y. Zhao, J. Tang, Z. Quan, Pressure-induced remarkable enhancement of self-trapped exciton emission in one-dimensional $CsCu_2I_3$ with tetrahedral units, J. Am. Chem. Soc. 142 (2020) 1786–1791, https://doi.org/10.1021/jacs.9b13419.
[30] Y. Li, Z. Shi, L. Wang, Y. Chen, W. Liang, D. Wu, X. Li, Y. Zhang, C. Shan, X. Fang, Solution-processed one-dimensional $CsCu_2I_3$ nanowires for polarization-sensitive and flexible ultraviolet photodetectors, Mater. Horiz. 7 (2020) 1613–1622, https://doi.org/10.1039/D0MH00250J.
[31] L. Lian, M. Zheng, P. Zhang, Z. Zheng, K. Du, W. Lei, J. Gao, G. Niu, D. Zhang, T. Zhai, S. Jin, J. Tang, X. Zhang, J. Zhang, Photophysics in $Cs_3Cu_2X_5$ (X = Cl, Br, or I): highly luminescent self-trapped excitons from local structure symmetrization, Chem. Mater. 32 (2020) 3462–3468, https://doi.org/10.1021/acs.chemmater.9b05321.
[32] Z. Ma, Z. Shi, C. Qin, M. Cui, D. Yang, X. Wang, L. Wang, X. Ji, X. Chen, J. Sun, D. Wu, Y. Zhang, X.J. Li, L. Zhang, C. Shan, Stable yellow light-emitting devices based on ternary copper halides with broadband emissive self-trapped excitons, ACS Nano 14 (2020) 4475–4486, https://doi.org/10.1021/acsnano.9b10148.
[33] L. Wang, Z. Shi, Z. Ma, D. Yang, F. Zhang, X. Ji, M. Wang, X. Chen, G. Na, S. Chen, D. Wu, Y. Zhang, X. Li, L. Zhang, C. Shan, Colloidal synthesis of ternary copper halide nanocrystals for high-efficiency deep-blue light-emitting diodes with a half-lifetime above 100h, Nano Lett. 20 (2020) 3568–3576, https://doi.org/10.1021/acs.nanolett.0c00513.
[34] F. Zhang, Z. Zhao, B. Chen, H. Zheng, L. Huang, Y. Liu, Y. Wang, A.L. Rogach, Strongly emissive lead-free 0D $Cs_3Cu_2I_5$ perovskites synthesized by a room temperature solvent evaporation crystallization for down-conversion light-emitting devices and fluorescent inks, Adv. Opt. Mater. 8 (2020), 1901723, https://doi.org/10.1002/adom.201901723.
[35] J. Lin, H. Chen, J. Kang, L.N. Quan, Z. Lin, Q. Kong, M. Lai, S. Yu, L.-L. Wang, M. F. Toney, P. Yang, Copper(I)-based highly emissive all-inorganic rare-earth halide clusters, Matter 1 (2019) 180–191, https://doi.org/10.1016/j.matt.2019.05.027.
[36] S. Hull, P. Berastegui, Crystal structures and ionic conductivities of ternary derivatives of the silver and copper monohalides—II: ordered phases within the (AgX)x–(MX)1−x and (CuX)x–(MX)1−x (M= K, Rb and Cs; X=Cl, Br and I) systems, J. Solid State Chem. 177 (2004) 3156–3173, https://doi.org/10.1016/j.jssc.2004.05.004.
[37] T. Li, X. Mo, C. Peng, Q. Lu, C. Qi, X. Tao, Y. Ouyang, Y. Zhou, Distinct green electroluminescence from lead-free $CsCuBr_2$ halide micro-crosses, Chem. Commun. 55 (2019) 4554–4557, https://doi.org/10.1039/C8CC09265F.
[38] P. Cheng, L. Sun, L. Feng, S. Yang, Y. Yang, D. Zheng, Y. Zhao, Y. Sang, R. Zhang, D. Wei, W. Deng, K. Han, Colloidal synthesis and optical properties of all-inorganic low-dimensional cesium copper halide nanocrystals, Angew. Chem. 131 (2019) 16233–16237, https://doi.org/10.1002/ange.201909129.
[39] R. Lin, Q. Guo, Q. Zhu, Y. Zhu, W. Zheng, F. Huang, All-inorganic $CsCu_2I_3$ single crystal with high-PLQY (≈ 15.7%) intrinsic white-light emission via strongly localized 1D excitonic recombination, Adv. Mater. 31 (2019), 1905079, https://doi.org/10.1002/adma.201905079.
[40] R. Roccanova, A. Yangui, G. Seo, T.D. Creason, Y. Wu, D.Y. Kim, M.-H. Du, B. Saparov, Bright luminescence from nontoxic $CsCu_2X_3$ (X = Cl, Br, I), ACS Mater. Lett. 1 (2019) 459–465, https://doi.org/10.1021/acsmaterialslett.9b00274.
[41] N.G. Park, Perovskite solar cells: an emerging photovoltaic technology, Mater. Today 18 (2015) 65–72, https://doi.org/10.1016/j.mattod.2014.07.007.
[42] A. Wojakowska, A. Górniak, A. Yu Kuznetsov, A. Wojakowski, J. Josiak, Phase diagram of the system copper(I) iodide + cesium iodide, J. Chem. Eng. Data 48 (2003) 468–471, https://doi.org/10.1021/je020188x.
[43] Y. Liu, Y. Zhang, K. Zhao, Z. Yang, J. Feng, X. Zhang, K. Wang, L. Meng, H. Ye, M. Liu, S.F. Liu, A 1,300 mm 2 ultrahigh-performance digital imaging assembly using high-quality perovskite single crystals, Adv. Mater. 30 (2018), 1707314, https://doi.org/10.1002/adma.201707314.
[44] K.L. Deutsch, B.H. Shanks, Active species of copper chromite catalyst in C–O hydrogenolysis of 5-methylfurfuryl alcohol, J. Catal. 285 (2012) 235–241, https://doi.org/10.1016/j.jcat.2011.09.030.
[45] Y. Peng, L. Shang, Y. Cao, G.I.N. Waterhouse, C. Zhou, T. Bian, L.Z. Wu, C.H. Tung, T. Zhang, Copper(i) cysteine complexes: efficient earth-abundant oxidation co-catalysts for visible light-driven photocatalytic H_2 production, Chem. Commun. 51 (2015) 12556–12559, https://doi.org/10.1039/C5CC04739K.
[46] H.J. Snaith, Present status and future prospects of perovskite photovoltaics, Nat. Mater. 17 (2018) 372–376, https://doi.org/10.1038/s41563-018-0071-z.
[47] D. Li, G. Wang, H.-C. Cheng, C.-Y. Chen, H. Wu, Y. Liu, Y. Huang, X. Duan, Size-dependent phase transition in methylammonium lead iodide perovskite microplate crystals, Nat. Commun. 7 (2016) 11330, https://doi.org/10.1038/ncomms11330.
[48] T. Baikie, Y. Fang, J.M. Kadro, M. Schreyer, F. Wei, S.G. Mhaisalkar, M. Graetzel, T. J. White, Synthesis and crystal chemistry of the hybrid perovskite $(CH_3NH_3)PbI_3$ for solid-state sensitised solar cell applications, J. Mater. Chem. A 1 (2013) 5628–5641, https://doi.org/10.1039/C3TA10518K.
[49] A. Dualeh, P. Gao, S.I. Seok, M.K. Nazeeruddin, M. Grätzel, Thermal behavior of methylammonium lead-trihalide perovskite photovoltaic light harvesters, Chem. Mater. 26 (2014) 6160–6164, https://doi.org/10.1021/cm502468k.
[50] R.J. Sutton, G.E. Eperon, L. Miranda, E.S. Parrott, B.A. Kamino, J.B. Patel, M. T. Hörantner, M.B. Johnston, A.A. Haghighirad, D.T. Moore, H.J. Snaith, Bandgap-tunable cesium lead halide perovskites with high thermal stability for efficient solar cells, Adv. Energy Mater. 6 (2016), 1502458, https://doi.org/10.1002/aenm.201502458.
[51] K. Wang, Z. Jin, L. Liang, H. Bian, D. Bai, H. Wang, J. Zhang, Q. Wang, S. Liu, All-inorganic cesium lead iodide perovskite solar cells with stabilized efficiency beyond 15, Nat. Commun. 9 (2018) 4544, https://doi.org/10.1038/s41467-018-06915-6.
[52] N. Mondal, A. De, A. Samanta, Achieving near-unity photoluminescence efficiency for blue-violet-emitting perovskite nanocrystals, ACS Energy Lett. 4 (2019) 32–39, https://doi.org/10.1021/acsenergylett.8b01909.
[53] V. Pinchetti, A. Anand, Q.A. Akkerman, D. Sciacca, M. Lorenzon, F. Meinardi, M. Fanciulli, L. Manna, S. Brovelli, Trap-mediated two-step sensitization of manganese dopants in perovskite nanocrystals, ACS Energy Lett. 4 (2019) 85–93, https://doi.org/10.1021/acsenergylett.8b02052.
[54] S. Liu, M. He, X. Di, P. Li, W. Xiang, X. Liang, $CsPbX_3$ nanocrystals films coated on YAG:Ce^{3+} PiG for warm white lighting source, Chem. Eng. J. 330 (2017) 823–830, https://doi.org/10.1016/j.cej.2017.08.032.
[55] Q. Dong, Y. Fang, Y. Shao, P. Mulligan, J. Qiu, L. Cao, J. Huang, Electron-hole diffusion lengths > 175 μm in solution-grown $CH_3NH_3PbI_3$ single crystals, Science 347 (2015) 967–970, https://doi.org/10.1126/science.aaa5760.
[56] Y. Liu, Z. Yang, D. Cui, X. Ren, J. Sun, X. Liu, J. Zhang, Q. Wei, H. Fan, F. Yu, X. Zhang, C. Zhao, S.F. Liu, Two-inch-sized perovskite $CH_3NH_3PbX_3$ (X = Cl, Br, I) crystals: growth and characterization, Adv. Mater. 27 (2015) 5176–5183, https://doi.org/10.1002/adma.201502597.
[57] Y. Fang, H. Wei, Q. Dong, J. Huang, Quantification of re-absorption and re-emission processes to determine photon recycling efficiency in perovskite single crystals, Nat. Commun. 8 (2017) 14417, https://doi.org/10.1038/ncomms14417.
[58] M.I. Saidaminov, A.L. Abdelhady, B. Murali, E. Alarousu, V.M. Burlakov, W. Peng, I. Dursun, L. Wang, Y. He, G. Maculan, A. Goriely, T. Wu, O.F. Mohammed, O. M. Bakr, High-quality bulk hybrid perovskite single crystals within minutes by inverse temperature crystallization, Nat. Commun. 6 (2015) 7586, https://doi.org/10.1038/ncomms8586.
[59] P.E. Blöchl, Projector augmented-wave method, Phys. Rev. B 50 (1994) 17953–17979, https://doi.org/10.1103/PhysRevB.50.17953.
[60] G. Kresse, J. Furthmüller, Efficient iterative schemes forab initiototal-energy calculations using a plane-wave basis set, Phys. Rev. B 54 (1996) 11169–11186, https://doi.org/10.1103/PhysRevB.54.11169.
[61] G. Kresse, D. Joubert, From ultrasoft pseudopotentials to the projector augmented-wave method, Phys. Rev. B 59 (1999) 1758–1775, https://doi.org/10.1103/PhysRevB.59.1758.
[62] Q.A. Akkerman, V. D'Innocenzo, S. Accornero, A. Scarpellini, A. Petrozza, M. Prato, L. Manna, Tuning the optical properties of cesium lead halide perovskite nanocrystals by anion exchange reactions, J. Am. Chem. Soc. 137 (2015) 10276–10281, https://doi.org/10.1021/jacs.5b05602.
[63] H. Liu, Z. Wu, J. Shao, D. Yao, H. Gao, Y. Liu, W. Yu, H. Zhang, B. Yang, $CsPbxMn_{1-x}Cl_3$ perovskite quantum dots with high Mn substitution ratio, ACS Nano 11 (2017) 2239–2247, https://doi.org/10.1021/acsnano.6b08747.
[64] H. Liu, Z. Wu, H. Gao, J. Shao, H. Zou, D. Yao, Y. Liu, H. Zhang, B. Yang, One-step preparation of cesium lead halide $CsPbX_3$ (X = Cl, Br, and I) perovskite nanocrystals by microwave irradiation, ACS Appl. Mater. Interfaces 9 (2017) 42919–42927, https://doi.org/10.1021/acsami.7b14677.